IEEE Access
Multidisciplinary | Rapid Review | Open Access Journal

Received November 4, 2020, accepted December 7, 2020, date of publication December 11, 2020,
date of current version December 31, 2020.

Digital Object Identifier 10.1109/ACCESS.2020.3044167

Wireless Channel Scene Recognition Method Based on an Autocorrelation Function and Deep Learning

SHUGUANG NING[1], YIGANG HE[2], LIFEN YUAN[1], YUAN HUANG[1], SHUDONG WANG[1], (Graduate Student Member, IEEE), TONGTONG CHENG[1], AND YONGBO SUI[1]

[1]School of Electrical Engineering and Automation, Hefei University of Technology, Hefei 230009, China
[2]School of Electrical Engineering, Wuhan University, Wuhan 430072, China

Corresponding authors: Yigang He (18655136887@163.com) and Lifen Yuan (yuanlifenhfut@163.com)

This work was supported in part by the National Key Research and Development Plan "Important Scientific Instruments and Equipment Development" under Grant 2016YFF0102200, in part by the National Natural Science Foundation of China under Grant 51977153, Grant 51977161, and Grant 51577046, in part by the State Key Program of National Natural Science Foundation of China under Grant 51637004, and in part by the Equipment Research Project in Advance under Grant 41402040301.

ABSTRACT Wireless channel scene recognition plays a key role in cognitive radio (CR) mobile communication systems. This paper proposes a wireless channel scene identification framework based on the autocorrelation function and deep learning. First, a feature extraction (FE) method is developed to perform a channel scene date analysis based on the autocorrelation function (AF). The AF is used to realize the FE method because it can be combined with Fourier transform (FT) to accurately extract the characteristics accurately from a time-varying channels scene. Second, a deep belief network (DBN) with a robust learning approach is introduced to perform wireless channel scene recognition. A novel learning architecture is employed, which combines the feature parameter and classification techniques to achieve a high classification correct recognition rate. Third, the k-step contrastive divergence (CD-k) algorithm is introduced as the preliminary training method to optimize the traditional DBN network. This method can effectively calculate the logarithmic gradient of the Boltzmann machine. Moreover, the up-down optimization algorithm is applied to optimize the network parameters. Finally, the theoretical implementation is described in detail, and the method is verified by constructing an experiment platform for an engineering application. The experimental results indicate that the proposed classifier is an excellent approach to realize channel scene recognition through advanced methods. The classification accuracy of the proposed approach is higher than that of several existing techniques.

INDEX TERMS Wireless channel, scene recognition, autocorrelation function, deep belief network (DBN).

I. INTRODUCTION

Cognitive radio has developed rapidly in recent years. The main goal is to achieve reliable communication by enhancing the spectrum utilization. To this end, the key step is to identify and analyse the scene of the wireless channels. In wireless communication, we call the different types of wireless channels models in different environments as wireless channel scenarios. After identifying the wireless channel scene, the physical layer technology suitable for the channel can be adapted to further enhance the performance of the communication system. However, the electromagnetic environment is complex, with diverse signals that change rapidly in the wireless communication domain [1], [2]. Moreover, the wireless channel environment involves large-scale fading [3], [4], small-scale fading [5], [6], and Doppler effects [7], [8]. Consequently, realizing scene recognition in wireless channels is challenging. In this scenario, it is necessary to adopt an advanced intelligent method to comprehensively identify the complex communication environments comprehensively. Therefore, the study of wireless channel scene recognition is of significance.

To solve the problem of the challenging identification in an additive noise channel environment, an unbiased blind

The associate editor coordinating the review of this manuscript and approving it for publication was Jenny Mahoney.

adaptive channel identification and equalization algorithm was proposed in [9]. The considered structural property can be observed in many array processing applications. Paper [10] recommended measures for non-line-of-sight (NLOS) identification, which is based on the space-time-frequency channel. This method can achieve a high recognition performance for line of sight (NLOS) and NLOS channels. To reduce the influence of noise in blind channel identification, a subspace tracking algorithm was proposed in [11], based on the recursive least squares (RLS) approach. However, RLS-based algorithms are widely known to be sensitive to the impulse noise in an actual scene. Paper [12] proposed a channel recognition scheme to overcome this dilemma, which based on the robust statistics subspace tracking method. However, this method is applicable for only three different types of time-varying channel scenarios. A blind channel identification method based on a weighted statistical mixture model was introduced in [13] for indoor scenario clustering. It is a weighted statistical mixture model [13]. However, this method is suitable for only for indoor wireless channel scenarios. In [14], a method to realize wireless channel classification was introduced to combine convolutional neural networks, and this technique was successfully applied to realize modulation recognition. In [15], the authors proposed a channel status classification approach by using the Received Signal Strength Indicator (RSSI) in indoor scenarios. The threshold was changed according to the statistical features in the special channel environment. This algorithm yielded a classification accuracy of approximately 85%.

However, in general, transmitters are located far away from the base station, and there are many reflectors are present. Consequently, no direct path exists between the transmitter and receiver, and the channel obeys a Rayleigh distribution [16]. Clarke first proposed the classical Clarke model for the Rayleigh time variation channel in [17]. Jakes optimized the Clarke model; however, the model could not maintain the stability of the broadband [18]. Thus, an improved model was proposed by Pop and Beaulieu [19]. In addition, certain channels have been proposed for different channel scenarios and research fields. In general, Research on the wireless channels can be examined through computer simulations and platform construction. The simulation models can be divided into deterministic and statistical models [20]. Deterministic models are also known as sum-of-sinusoids methods, in which the key aspect is to simulate the characteristics of the fading channel by superposing a large number of sinusoidal signals with different information. In the statistical models is also known as the formed filter methods [21], the power spectral density is modified through white Gaussian noise to simulate different wireless channel scenarios.

In recent years, artificial intelligence has been widely developed, and pattern recognition method based on neural network has been widely used. Wireless channel recognition based on neural network mainly includes feature extraction and classification recognition. A wireless channel often exhibits randomness and time variability, which increases the difficulty of extracting the wireless channel feature extractions. Certain researchers [22] used the wavelet transform technology to extract the fingerprint features of a wireless network. Moreover, an array-based feature extraction method was proposed to determine the radio frequency fingerprint [23]. The characteristic parameters were estimated considering the rotation invariance. The feature extraction functions usually involve a Fourier transform [24], Hilbert transform [25], linear discriminant analysis [26], principal component analysis [27], or other dimensionality reduction techniques [28]. However, it is difficult to extract the characteristic parameters of channel scenes. In this paper, a feature parameter extraction method based on the autocorrelation function is proposed. The power spectral density with more robust characteristics can be obtained by combining the autocorrelation function with Fourier transform, and PSD has more vital characteristic attributes. To realize channel scene recognition, after extracting the characteristic parameters the classification algorithm should be employed. The existing classification and recognition methods can be divided into two categories: decision theory-based methods and pattern recognition methods [29], [30]. The identification problem is considered to be a compound hypothesis test problem based on the decision theory, and an appropriate threshold value is selected as the decision basis. For example, the power weighted statistical model applied is a decision-theory-based method to realize indoor wireless channel scene clustering [31]. However, this method cannot be widely applied owing to its complicated derivation and high operation cost. Methods based on pattern recognition can be roughly divided into neural network methods [32], radial basis neural network methods (RBF) [33], support vector machine methods (SVM) [34], and multiple kernel relevance vector machine (MKRVM) techniques [35]. These methods have been widely used in classification and recognition tasks. However, in the wireless channel scenarios with fast time-variations, large broadband, and multiple-dimensions, these traditional methods cannot achieve high recognition accuracy. To enhance the identification effect, this article proposes a wireless channel scene classification method based on a deep learning network. Compared with the traditional neural network method, the pattern recognition method based on deep learning has more vigorous learning and classification ability.

A new scene recognition method mainly includes two processes: feature extraction and classification based on the AF and DBN, respectively. The key contributions of this paper can be summarized as follows.

(1) A feature extraction method based on the AF is proposed for a wireless channel based on AF. The AF is derived through the complex baseband impulse response in the wireless channel. The characteristic parameters are obtained by using the AF combined with a Fourier transform. In particular, a Fourier transform, windowing, and normalization are realized to achieve high quality characteristic parameters.

(2) A method is proposed to realize wireless channel scene recognition based on a DBN. This method constructs a hybrid classifier model by using the Boltzmann machine. The model includes both undirected and directed parts.

(3) The training of deep learning networks is realized using two processes, specifically, non-supervised pre-training and supervised parameter tuning. The CD-k learning algorithm is used to optimize the DBN network to promptly calculate the log-likelihood gradient of the constrained Boltzmann machine. The upper and lower algorithms are adopted to avoid large deviation during classification.

4) Two approaches are employed to verify the correctness and accuracy of the proposed method. One method is to obtain the Rayleigh fading channel of different scenarios through the forming filter method, and then the channel recognition is realized using the proposed approach. The other method is to build a wireless channel scene simulation platform by combining hardware and software. Subsequently, the proposed method in this paper is used to test and verify the wireless channel scene data collected by the platform.

The remaining paper is arranged as follows. In Section II, describes the Rayleigh time-varying channel and the process of feature parameter extraction, along with the DBN network. The DBN design and model structure of the recognition algorithm are described in Section III. The experiment and results analysis are presented in Section IV. Specifically, the section involves two parts. Part one corresponds to the channel simulation and method verification, and part two corresponds to the experiment platform and results in analysis of the results. Section V presents the concluding remarks.

II. RAYLEIGH TIME VARIATION CHANNEL AND FEATURE PARAMETER EXTRACTION

First, we describe the Rayleigh time variation channel, followed by the solution of the autocorrelation algorithm in the wireless domain. Subsequently, we describe the process of the feature parameters extraction by using the autocorrelation algorithm.

A. RAYLEIGH TIME VARIATION CHANNEL

In this section, we describe the modelling of the time-dependent channel variation with the movement of the mobile terminal. The actual environment is shown in Fig.1. A plane wave arrives at an angle. Suppose that a station moves at a certain velocity, and the wave arrives $x \rightarrow y$ horizontally in the plane.

When $x(t)$ is the baseband transmitting signal, the corresponding baseband transmitting signal is:

$$\tilde{x}(t) = \mathrm{Re}\left[x(t)\, \mathrm{e}^{\mathrm{j}2\pi f_c t}\right] \tag{1}$$

where, $\mathrm{Re}[(t)]$ represents the real part.

Given a velocity υ and wavelength λ, the Doppler frequency shift can be defined as

$$f_i = f_D \cos\theta_i = \frac{v}{\lambda}\cos\theta_i \tag{2}$$

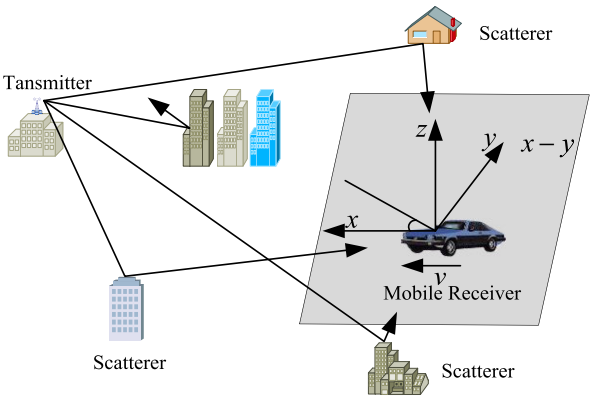

FIGURE 1. Non-line-of-sight communication environment.

where, f_D is the maximum Doppler shift, and θ_i is the angle of arrival (AOA) corresponding to the *ith* plane wave.

After the baseband transmitting signal passes the scattering channel through a strip propagation path, the received signal in the passband can be expressed as

$$\tilde{y}(t) = \mathrm{Re}\left[y(t)\, e^{\mathrm{j}2\pi f_c t}\right] = \mathrm{Re}\left[\sum_{i=1}^{I} C_i \mathrm{e}^{-j\phi_i(t)} x(t-\tau_i)\, \mathrm{e}^{\mathrm{j}2\pi f_c t}\right] \tag{3}$$

where, $y(t)$ is the baseband signal; C_i and τ_i respectively represent the channel gain and delay of the f_i propagation path; f_i represents the Doppler frequency shift, with $\phi_i(t) = 2\pi\{(f_c + f_i)\tau_i - f_i\tau_i\}$. Therefore, the baseband signal can be modelled as a linear time-varying filter, as in formula (3), and the complex baseband impulse response can be defined as follows:

$$h(t,\tau) = \sum_{i=1}^{I} C_i \mathrm{e}^{-\mathrm{j}\phi_i(t)} \delta(t, \tau_i) \tag{4}$$

where, $\delta_i(\cdot)$ is the Dirac delta function. When the sampling period T_s is considerably larger than the path delay difference, the path delay τ_i can be approximated as $\tilde{\tau}$.

Therefore, equation (4) can be expressed as

$$h(t,\tau) = h(t)\,\delta(t-\tilde{\tau}) \tag{5}$$

In this case, $h(t) = \sum_{i=1}^{I} C_i \mathrm{e}^{-\mathrm{j}\phi_i(t)}$. When the baseband transmitting signal $x(t) = 1$, the passband receiving signal is

$$\begin{aligned}\tilde{y}(t) &= \mathrm{Re}\left[y(t)\,\mathrm{e}^{\mathrm{j}2\pi f_c t}\right] = \mathrm{Re}\left[\left\{h_I(t) + \mathrm{j}h_Q(t)\right\}\mathrm{e}^{\mathrm{j}2\pi f_c t}\right] \\ &= h_I(t)\cos(2\pi f_c t) + h_Q(t)\sin(2\pi f_c t)\end{aligned} \tag{6}$$

where $h_I(t) = \sum_{i=1}^{I} C_i(t)\cos\phi_i(t)$ is the coaxial component, $h_Q(t) = \sum_{i=1}^{I} C_i(t)\sin\phi_i(t)$ is the orthogonal component, ϕ_0 is the phase offset, and $\phi_i(t) == 2\pi f_c \tau_i(t) - \phi_{D_i} - \phi_0$ is the delay.

If I is sufficiently large, the central limit theorem can be used to approximate $h_I(t)$ and $h_Q(t)$ jointly as Gaussian

random processes. The Gaussian property holds for I when the $\phi_i(t)$ is evenly distributed on $[-\pi, \pi]$, and $C_i(t)$ obeys the Rayleigh distribution.

B. AUTOCORRELATION FUNCTION FOR WIRELESS CHANNELS

In this paper, the autocorrelation algorithm is used to extract the characteristic parameters in different channel scenarios. We use $h_I(t)$ and $h_Q(t)$ to represent the in-phase and quadrature received signal components, respectively. Our derivations are based on certain key assumptions which are applied to different Rayleigh channel models. The multipath is defined as $\tau_i(t)$, is defined as C_i, and Doppler frequency is defined as $f_{D_i}(t)$. We assume that these parameters change gradually and can be considered as constants for a brief period. Thus, $C_i(t) \approx C_i$, $f_{D_i}(t) \approx f_{D_i}$, and $\tau_i(t) \approx \tau_i$. Therefore, $\phi_{D_i}(t) = \int_t 2\pi f_{D_i} dt = 2\pi f_{D_i} t$. In this case, the phase is $\phi_i(t) = 2\pi f_c \tau_i - 2\pi f_{D_i} t - \phi_0$. Thus,

$$\begin{aligned} \mathrm{E}[h_I(t)] &= \mathrm{E}\left[\sum_i C_i \cos\phi_i(t)\right] \\ &= \sum_i \mathrm{E}[C_i]\mathrm{E}[\cos\phi_i(t)] = 0 \end{aligned} \tag{7}$$

where the equality indicates that the C_i and $\cos\phi_i(t)$ are independent, and follows from the uniform distribution pertaining to ϕ_i. Similarly, as we can prove that $\mathrm{E}\left[h_Q(t)\right] = 0$. Therefore, considering the autocorrelation of the h_I and h_Q, we can obtain the following expression:

$$\begin{aligned} \mathrm{E}\left[h_I(t)\, h_Q(t)\right] &= \sum_i \sum_j \mathrm{E}\left[C_i C_j\right] \mathrm{E}\left[\cos\phi_i(t) \sin\phi_j(t)\right] \\ &= \sum_i \mathrm{E}\left[C_i^2\right] \mathrm{E}[\cos\phi_i(t) \sin\phi_i(t)] = 0 \end{aligned} \tag{8}$$

Thus, $h_I(t)$ and $h_Q(t)$ are uncorrelated, since these two variables are Gaussian processes.

We can obtain the autocorrelation $A_{h_I}(t, \tau)$ if following a similar derivation from formula (8).

$$\begin{aligned} A_{h_I}(t, \tau) &= \mathrm{E}[h_I(t)\, h_I(t+\tau)] \\ &= \sum_i \mathrm{E}\left[C_i^2\right] \mathrm{E}[\cos\phi_i(t) \cos\phi_i(t+\tau)] \end{aligned} \tag{9}$$

By substituting $\phi_i(t) = 2\pi f_c \tau_i - 2\pi f_{D_i} t - \phi_0$ and $\phi_i(t+\tau) = 2\pi f_c \tau_i - 2\pi f_{D_i}(t+\tau) - \phi_0$ in formula (7), we can obtain

$$\begin{aligned} &\mathrm{E}[\cos\phi_i(t) \cos\phi_i(t+\tau)] \\ &= 5\mathrm{E}\left[\cos\left(2\pi f_{D_i}\pi\right)\right] \\ &\quad + 5\mathrm{E}\left[\cos\left(4\pi f_c \tau_i - 4\pi f_{D_i} t - 2\pi f_{D_i}\tau - 2\phi_0\right)\right] \end{aligned} \tag{10}$$

Since $2\pi f_c \tau_i$ changes rapidly and is uniformly distributed, so the second expectation part in (10) becomes zero. Therefore,

$$\begin{aligned} A_{h_I}(t, \tau) &= 5\sum_i \mathrm{E}\left[C_i^2\right] \mathrm{E}[\cos(2\pi f_D \tau)] \\ &= 5\sum_i \mathrm{E}\left[C_i^2\right] \cos(2\pi v\tau \cos\theta_i/\lambda) \end{aligned} \tag{11}$$

Assume that $f_{D_i} = v\cos\theta_i/\lambda$ is fixed. Since $A_{h_I}(t, \tau) = A_{h_I}(\tau)$, and $A_{h_I}(t, \tau)$ depends only on τ, thus $h_I(t)$ is a wide-sense stationary random process.

A similar derivation yields similar results for the $h_Q(t)$ autocorrelation as $h_I(t) = h_Q(t)$. The cross-correlation between the $h_I(t)$ and $h_Q(t)$ can be expressed as

$$\begin{aligned} A_{h_I,h_Q}(t, \tau) &= A_{h_I,h_Q}(\tau) \\ &= \mathrm{E}\left[h_I(t)\, h_Q(t+\tau)\right] \\ &= -5\sum_i \mathrm{E}\left[C_i^2\right] \sin(2\pi v\tau \cos\theta_i/\lambda) \\ &= -\mathrm{E}\left[h_Q(t)\, h_I(t+\tau)\right] \end{aligned} \tag{12}$$

Thus $\tilde{y}(t) = h_I(t)\cos(2\pi f_c t) + h_Q(t)\sin(2\pi f_c t)$ is also wide-sense stationery (WSS), and

$$\begin{aligned} A_h(\tau) &= \mathrm{E}[h(t)\, h(t+\tau)] \\ &= A_{h_I}(\tau)\cos(2\pi f_c \tau) + A_{h_I,h_Q}(\tau)\sin(2\pi f_c \tau) \end{aligned} \tag{13}$$

We consider certain assumptions to simplify (11) and (12) in the context of the wireless communication environment, with the emphasis on ensuring a uniform scattering environment. We assume the angle of arrival of the multipath scattering components, $\theta_n = i\Delta\theta$, where $\Delta\theta = 2\pi/N$, and hypothesize that each multipath component has the identical received power, therefore $\mathrm{E}\left[C_i^2\right] = 2P_h/N$. P_h is the received power. In this case, (13) can be expressed as

$$\begin{aligned} A_h(\tau) &= \mathrm{E}[h(t)\, h(t+\tau)] \\ &= A_{h_I}(\tau)\cos(2\pi f_c \tau) + A_{h_I,h_Q}(\tau)\sin(2\pi f_c \tau) \end{aligned} \tag{14}$$

We substitute $N = 2\pi/\Delta\theta$ into formula (14), and consider the limit of the number $N \to \infty$, and $\Delta\theta \to 0$. In this case then the summation in (14) can be expressed as an integral in (15).

$$A_{h_I}(\tau) = \frac{P_h}{2\pi} \int \cos(2\pi v\tau \cos(\theta/\lambda))\, d\theta = P_h J_0(2\pi f_D \tau) \tag{15}$$

where $J_0(x) = \frac{1}{\pi}\int_0^{\pi} e^{-jx\cos\theta} d\theta$ is a Bessel function.

Similarly, we obtain the autocorrelation $A_{h_I,h_Q}(\tau)$ of a uniform scattering environment.

$$A_{h_I,h_Q}(\tau) = \frac{P_h}{2\pi} \int \sin(2\pi v\tau \cos(\theta/\lambda))\, d\theta = 0 \tag{16}$$

C. FEATURE PARAMETERS EXTRACTION THROUGH AUTOCORRELATION

The power spectral density (PSD) of $h_I(t)$ and $h_Q(t)$ can be expressed as by $S_I(f)$ and $S_Q(f)$, respectively, acquired by the Fourier transform of the corresponding autocorrelation functions. Since the autocorrelation functions are equal, they

have the same PSD. Thus, the PSD of the in-phase received signal components can be expressed as

$$S_{h_I}(f) = \mathcal{F}\left[A_{h_I}(\tau)\right] = \begin{cases} \dfrac{P_h}{2\pi f_D} \dfrac{1}{\sqrt{1-\left(\frac{f}{f_D}\right)^2}}, & |f| \le f_D \\ 0, & |f| > f_D \end{cases} \tag{17}$$

The PSD of the received signal $\tilde{y}(t)$ is obtained using formula (13), with $A_{h_I,h_Q}(\tau) = 0$, and the properties of the Fourier transform are used to determine the DSP formula of the classical model.

$$\begin{aligned} S_h(f) &= \mathcal{F}[A_h(\tau)] = 25\left[S_{h_I}(f-f_c) + S_{h_I}(f+f_c)\right] \\ &= \begin{cases} \dfrac{P_h}{4\pi f_D} \dfrac{1}{\sqrt{1-\left(\frac{|f-f_c|}{f_D}\right)^2}}, & |f-f_c| \le f_D \\ 0, & \text{else} \end{cases} \end{aligned} \tag{18}$$

where f_D is the maximum Doppler frequency shift. $f_D = f_c \cdot (v/c)$, where f_c is the carrier frequency, v is the vehicle speed, and c is the velocity of light.

Following a similar derivation, the DSP can be theoretically obtained for other kinds for Rayleigh time-varying channels.

The DSP formula of a flat fading channel is expressed by

$$S_h(f) = \frac{P_h}{2f_D}, \quad -f_D \le f \le f_D \tag{19}$$

The DSP expression of the Rayleigh Gaussian channel can be expressed as

$$S_h(f) = \frac{P_h}{\sqrt{2\pi\sigma_g^2}} e^{-\frac{f^2}{2\pi\sigma_g^2}}, \quad -f_D \le f \le f_D \tag{20}$$

where σ_g is the statistical variance of f_D.

The DSP formula of the rounded fading channel can be expressed as

$$S_h(f) = P_h\left[a_0 + a_2 * \left(\frac{f}{f_D}\right)^2 + a_4 * \left(\frac{f}{f_D}\right)^4\right] \tag{21}$$

where the coefficients a0, a2, and a4 correspond to the polynomial, Polynomial = [a0 a2 a4], which is a finite real vector, where $-f_D \le f \le f_D$.

The DSP expression of the Butterworth fading channel can be expressed

$$S_h(f) = \frac{P_h}{\pi f_D \sqrt{1-\left(\frac{f}{f_D}\right)^2}}, \quad -f_D \le f \le f_D \tag{22}$$

The PSD corresponds to the difference in the five different channels, determined by the Fourier transform of the corresponding AF respectively. Thus, the PSD can be used as a characteristic parameter to identify the different channel scenes.

III. DBN DESIGN AND MODEL STRUCTURE OF THE WIRELESS CHANNEL RECOGNITION ALGORITHM

This section describes the design of the DBN networks classifier, and channel scene recognition algorithm.

A. DESIGN OF THE DEEP BELIEF NETWORKS CLASSIFIER

The DBN network established in this paper is a hybrid model network, as shown in Fig.2. The top two layers are undirected graphs that form an associative memory network, and while the other layers form a directed graph. From the bottom up, a visible vector and the hidden layer vector $h_k = \left(h_{k,1}, h_{k,2}, \cdots h_{k,n}\right)^{\mathrm{T}}$ are present G^1, and the recognition weight is represented by W^1. $k = 1, 2, \cdots, r$. r represents the number of layers.

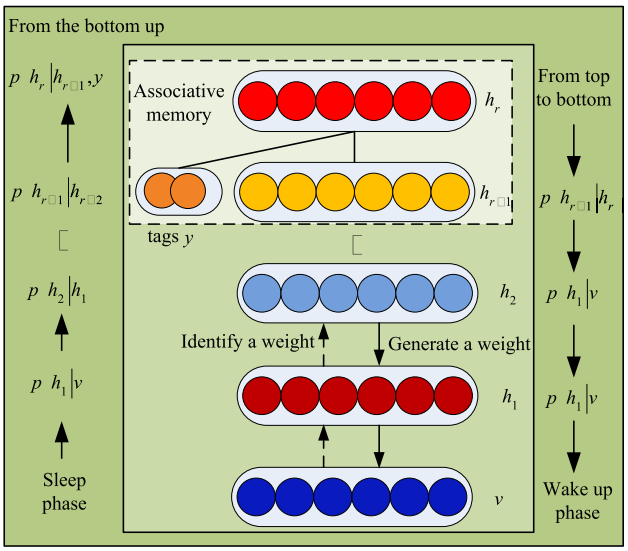

FIGURE 2. The architecture of the DBN.

The generated weights between the $(k-1)$ hidden layer and the f_D hidden layer are denoted as G^k, and the recognition weights are represented as W^k. However, the associative memory constitutes an undirected connection between the $(r-1)$ hidden layer and the r hidden layer, the connection weights between these layers are known as associative weights W^r. The bias is represented by the visible layer, and the generation bias is represented as b_k. Identification offset is represented as b^k. $(1 \le k \le r-1)$, and b^{r+1} is the identification offset of the label layer.

The joint probability distribution of the DBN can be expressed as

$$\begin{aligned} &p(v, y, h_1, h_2, \cdots, h_r|\theta) \\ &= p(v|h_1)\, p(h_1|h_2) \cdots p(h_{r-2}|h_{r-1})\, p((y, h_{r-1}), h_r) \end{aligned} \tag{23}$$

Parameter set $\theta = \left\{W^k, G^k, b^k, b_k, W^r, b^r, W^{r+1}, b^{r+1}, a\right\}$.

Moreover, $p((y, h_{r-1}), h_r)$ is computed as a constrained Boltzmann machine, (y, h_{r-1}) is the visible vector, and h_r is the implicit vector.

Using the probability sum technique to eliminate the label vector, the marginal distribution can be obtained as

$$p(v, y, h_1, h_2, \cdots, h_r \,|\theta) = p(v \,|h_1)\, p(h_1 \,|h_2) \cdots p(h_{r-1}, h_r) \quad (24)$$

The output classification probability can be calculated by using the maximum flexible output function:

$$p(y = e_i \,|h_i) = soft\max_i \left(W^{r+1} h_r + b^{r+1}\right) \quad (25)$$

For the remaining layers, there are

$$p(h_{k-1} \,|h_k) = \prod_i p\left(h_{k-1,i} \,|h_k\right), \quad \forall 1 \le k \le r-1 \quad (26)$$

B. CHANNEL SCENE RECOGNITION ALGORITHM

Compared with general classifiers, the DBN network exhibits a stronger deep representation ability and can effectively solve classification problems well. Therefore, this paper employs a deep learning network.

Algorithm 1 Learning Algorithm of DBN

Step 1: numbers close to 0, where $1 \le i \le r+1$.
Step 2: Using the CD-k algorithm to train the first RBM, the visual layer of the RBM is v and the hidden layer is h_1.
Step 3: For $1 \le i \le r-1$, take h_{i-1} as the visual layer of the ith RBM and h_i as the hidden layer of the ith RBM, use the CD-k algorithm to train the RBM layer by layer.
Step 4: For $i = r$, taking the whole of h_{r-1} and y as the visual layer and h_r as the hidden layer, construct a classifier RBM, and use the label CD-k algorithm for training.
Step 5: The pre-trained DBN is expanded into a deep perceptron.
Step 6: The up-down optimization algorithm is used to optimize the network parameters.
Step7: Stop training when the error meets the requirements.

In the unsupervised pre-training phase, the two adjacent layers (h_{k-1}, h_k) are treated as an RBM of the deep belief network with no labels. Moreover, the top two layers are treated as classification constrained Boltzmann machines, trained using CD-k algorithm to initialize a, W^k, G^k, b^k, and W^r, b^r, W^{r+1}, and b^{r+1}. The training process is aimed at using the conditional probabilities $Q(h_k \,|h_{k-1})$ and $Q(h_r \,|h_{r-1}, y)$ of these constrained BMs to estimate the conditional probabilities $p(h_k \,|h_{k-1}) \approx Q(h_k, h_{k-1})$ and $p(h_r \,|h_{r-1}, y) = Q(h_r \,|h_{r-1}, y)$, respectively.

In the up-down optimization phase, the recognition weights $G^k = \left(W^k\right)^{\mathrm{T}}$ are used to initialize the generated weights. All the networks are then tuned using the upper and lower algorithms. The up-down algorithm is a variation of the waking algorithm, which consists of waking and sleeping stages, as shown in Fig.2.

The learning discrimination process of the DBN is as algorithm 1. Step 1 - step 4 is the unsupervised training stage. Step 5 - step 7 is the supervised tuning phase.

In the sleep phase, to estimate the generation weights and generate offsets using the recognition weights and recognition bias are used repeatedly. The wake phase is aimed at realizing overall tuning according to the estimated recognition weight and identification bias.

In step 5, in the supervised tuning phase, the DBN is first expanded into a deep perceptron. The weight and bias are initialized using W^k, b^k, respectively, trained layer by layer in the deep perceptron, and through the back-propagation algorithm to optimize the global network. Moreover, the back-propagation algorithm is used to optimize the overall adjustment.

The overall architecture of the DBN based classification is shown in Fig.3. The architecture involves four major parts, a wireless channel, feature extraction, deep learning network construction and training, and classification.

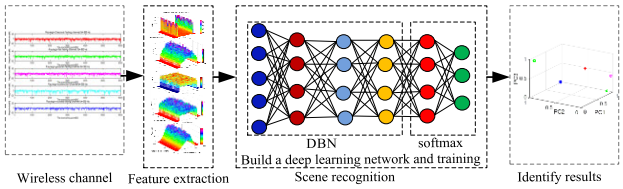

FIGURE 3. The overall architecture of the DBN based classification.

IV. EXPERIMENT AND ANALYSIS RESULTS

This section describes the experiment and the results of the recognition method based analysis. This section consists of two parts. The first part corresponds to the channel simulation and method verification, and the second part describes the experiment platform and results in analysis results.

Considering the static or quasi-static nature of the indoor channel, outdoor channels can be typically characterized according to the time variation of the channel gain, which depends on the mobile platform. The outdoor channel is mostly characterized by a Doppler spectrum that governs the time variation in the channel gain. In this paper, channel scenarios are examined through two paths of the theoretical simulation and channel simulator. The method is applied to the simulated and the measured channels pertaining to the feature extraction and classification, respectively. This part is divided into two subparts. Section A describes the implementation of the proposed method of this paper through a simulation experiment. Section B describes the accuracy validation of the proposed channel scenario platform.

A. WIRELESS CHANNEL SCENE AND VERIFICATION OF THE RECOGNITION METHOD

The simulation methods of the Rayleigh fading channel include the sine wave superposition method and forming filter method. Although the formed filter method has a high design complexity, its statistical accuracy is higher than that of the sinusoidal superposition method, and it can better simulate

the fading channel model. In this paper, the Doppler filter method is used to generate Rayleigh fading channel, and the channel implementation model is shown in Fig.4.

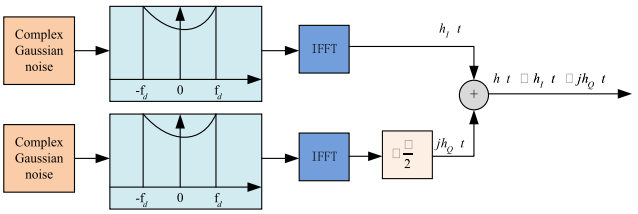

FIGURE 4. The wireless channel simulation model.

The channel model is devised under the assumption that the scattering components around a mobile station are uniformly distributed with an equal power for each component. Fig.4 shows the block diagram for the channel model, involving two branches, one branch corresponds to the real part, and the other branch corresponds to the imaginary part. In each branch, a complex Gaussian noise is first generated in the frequency domain and filtered by a Doppler filter such that the frequency component is subject to the Doppler shift. Finally, the Doppler-shifted Gaussian noise is transformed into the time-domain signal through an IFFT block. Since the output of the IFFT block must be a real signal, its input must always be conjugate symmetric. By constructing a complex channel gain by adding a real part to the imaginary part of the output, a channel following the Rayleigh distribution can be generated.

1) RELATED PARAMETER SETTINGS IN THE RAYLEIGH WIRELESS CHANNEL SCENE SIMULATION

Sample rate $= 10^4$; random number seed $=$ 'm19937ar with seed'; seed $= 34$; maximum Doppler shift $f_D = 500$ Hz; channel length $= 6000$ (function calls the impulse response points of a channel); The Gaussian parameters $\sigma_g^2 = 0.7071$; The cycle number of channel produces $= 20$; The length of the window function is 100, and the overlap number for each segment is window*3/4; The waveforms of the five kinds of simulated channels are shown in Fig. 5.

2) CHANNEL ASSESSMENT

Mutual movement occurs between the transmitter and receiver. The time-varying characteristics correspond to the scattering multipath channel, and the amplitude sum is the time-varying aspect of the in-phase component and the orthogonal component, which belong to the received signal. It has been proved that the Rayleigh distribution can be applied when the multipath number I is sufficiently large enough. This characteristic is used to evaluate the simulation channel model.

According to the definition of the Rayleigh distribution, the amplitude of PDF ($p(\tilde{y})$) should obey amplitude (27) belongs to the received signal $\tilde{y}(t)$:

$$p(\tilde{y}) = \frac{\tilde{y}}{\sigma^2} \exp\left(-\frac{\tilde{y}^2}{2\sigma^2}\right) \tag{27}$$

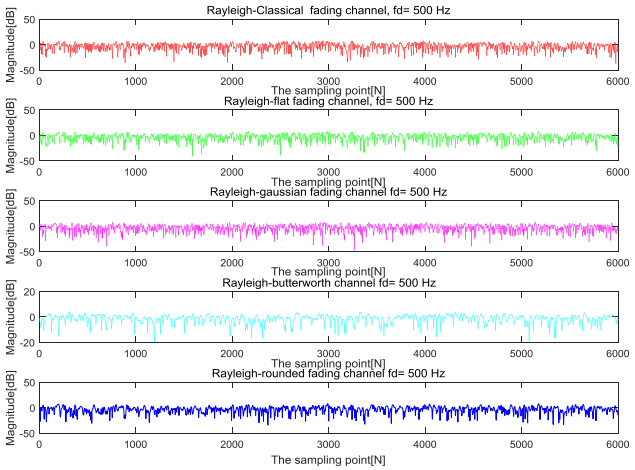

FIGURE 5. The waveforms of the five simulation.

When $f_D = 500\,Hz, T_s = 50\,[\mu s]$ is statistically the envelope of the received signal $\tilde{y}(t)$.

The probability statistics method is used to calculate the amplitude in the five channels. The channel validation results are shown in Fig.6. All five channels exhibit Rayleigh channel characteristics. Equations (16) indicate that $h_I(t)$ and $h_Q(t)$ are simultaneously independent of each other at the same time. When $f_D = 500$Hz, $T_s = 50\,[\mu s]$, and statistical analysis was conducted considering the phase of the different channel scenarios. The statistical results are shown in Fig.6 (b). The results indicate that all five channels exhibit a Rayleigh distribution.

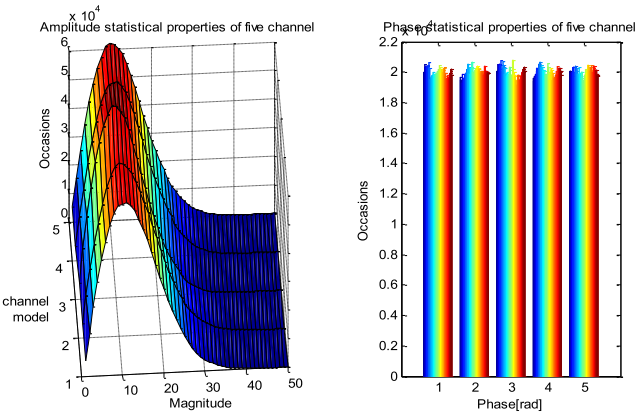

FIGURE 6. The statistical distribution of five different channel scenarios. (a) Amplitude statistical properties of five different channels. (b) Phase statistical properties of five different channels.

Five hundred Monte Carlo simulations were performed for each channel. The extraction method was used to extract the feature parameter for the five channels in this paper. The PSD functions were obtained for the in different channels. Fig.7 shows the 200 groups characteristic parameters obtained using the Monte Carlo method in four kind channels. The X-, Y-, and Z-axes show the Doppler frequency, experiment number and power of the PSD, respectively.

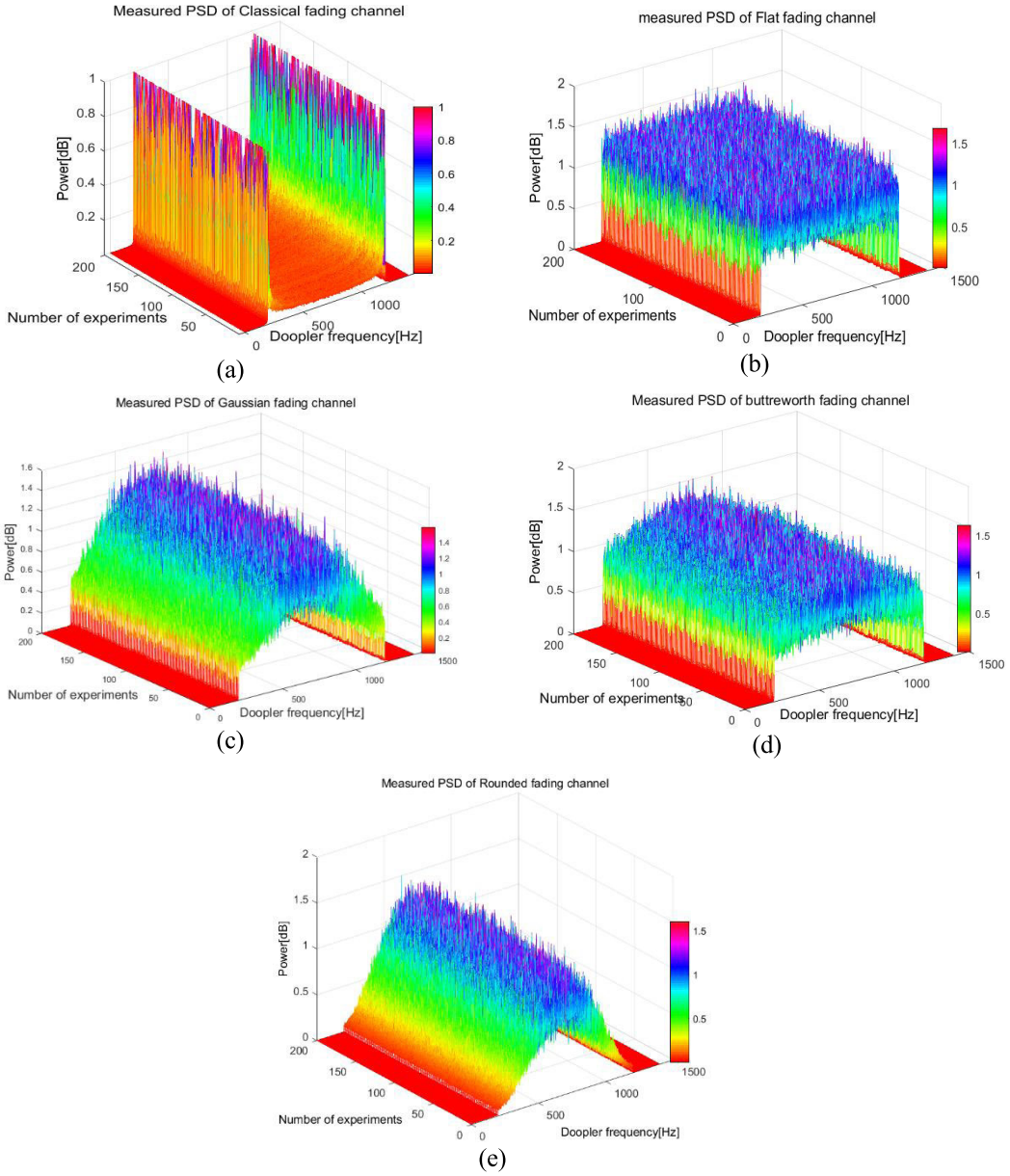

FIGURE 7. **The feature parameters extracted results by the autocorrelation method in different channel scenarios. (a) PSD in Classical fading channel. (b) PSD in Flat fading channel. (c) PSD in the Gaussian fading channel. (d) PSD in the Butterworth fading channel. (e) PSD in the Rounded fading channel.**

Fig.7 indicates that the characteristic parameters are significantly different in different channel scenarios. The extracted feature parameters can represent the essential features of varying channel scenes. The proposed method can be noted to be highly effective, and the extracted feature parameters can be used as training data for the DBN.

Parameter setting of the DBN: The number of nodes in the input layer is 1401. Three hidden layers exist 12-8-6-4, the softmax is set to have five nodes in the output layer, and the learning rate and penalty factor are set as 0.1 and 0.1, respectively. For each layer, the activation function adopts the sigma function. The number of pre-training iterations is 400, set to be 100 times of the fine-tuning iterations.

The results of the proposed method were compared with those of the BP neural network method, support vector machine (SVM) method, and Radial Basis Function (RBF) neural network method.

The number of nodes in the input layers and output layer of these three recognition methods was the same as those of the proposed DBN. The training and testing data of all the methods were the same, and several classification methods were trained and tested. During the training process, we performed the manual tuning of several methods. To present the comparative results more objectively, the final relevant experimental parameters of the identification methods are presented.

The hidden layer structure of the BP neural network corresponded to 128-4. The learning rate of the BP was 0.1, and the training accuracy was 10^{-3}. The BP was trained through the adaptive gradient descent method, and training da was used as the training function. The optimal parameter (penalty factor) of the SVM was obtained through cross-validation. The kernel function of the SVM was the radial basis function, and the training accuracy of the SVM was set as 10^{-3}. The RBF neural network was built automatically using the Newrbe function in MATLAB. The spread of the radial basis functions was set as 0.5. The Gaussian function was selected as the transfer function of the RBF neural network. The two-dimensional feature distribution is shown in Fig.8.

Fig.8 (a) shows the two-dimensional feature distribution diagram results obtained using the back-propagation (BP) neural network. As shown in Fig.8 (a), the curves for the Gaussian channel and rounded channel are partially overlapped, indicating that these curves cannot be well differentiated by the BP neural method. Moreover, the flat channel and Butterworth channel exhibit results that are overlapped to a certain extent, indicating that the neural network method had a mediocre performance in the recognition task.

Fig.8 (b) shows the effect of the application of the SVM neural network method in the scene recognition task. The three channels overlapped to different degrees from the two-dimensional feature diagram. This result indicates that the method cannot well distinguish the Gaussian channel from the rounded and Butterworth channels.

Fig.8 (c) shows the two-dimensional feature distribution diagram for the scene recognition based on the RBF neural network. Although this method can effectively classify the rounded, classical, and Gaussian channels, a considerable overlap occurs between the flat channel and Butterworth channel. This method cannot effectively identify the two-channel scenarios.

Fig. 8 (d) shows the two-dimensional feature distribution diagram corresponding to the proposed method. The two-dimensional features exhibit a notable degree of differentiation for the different channel scenes. No overlap occurs between the different channels, which indicates that this method exhibits a satisfactory scene recognition effect.

To clearly illustrate the recognition effect for different methods in the simulation channel environment. Table 1 presents the correct recognition rates for the four different scene recognition methods.

Table 1 indicates that the optimal channel scene recognition corresponds to the proposed method, which has a theoretical correct recognition rate of 100%. The BP neural network based method has the worst recognition effect, with a correct recognition rate of only 72.6%. The results of SVM and RBF results are comparable, with the correct recognition rates of 82.4% and 87.4%, respectively. The theoretical experimental results show that the proposed DBN method has a more powerful learning ability than the other methods. The proposed deep learning method exhibits a better representation and classification ability in terms of the channel characteristics.

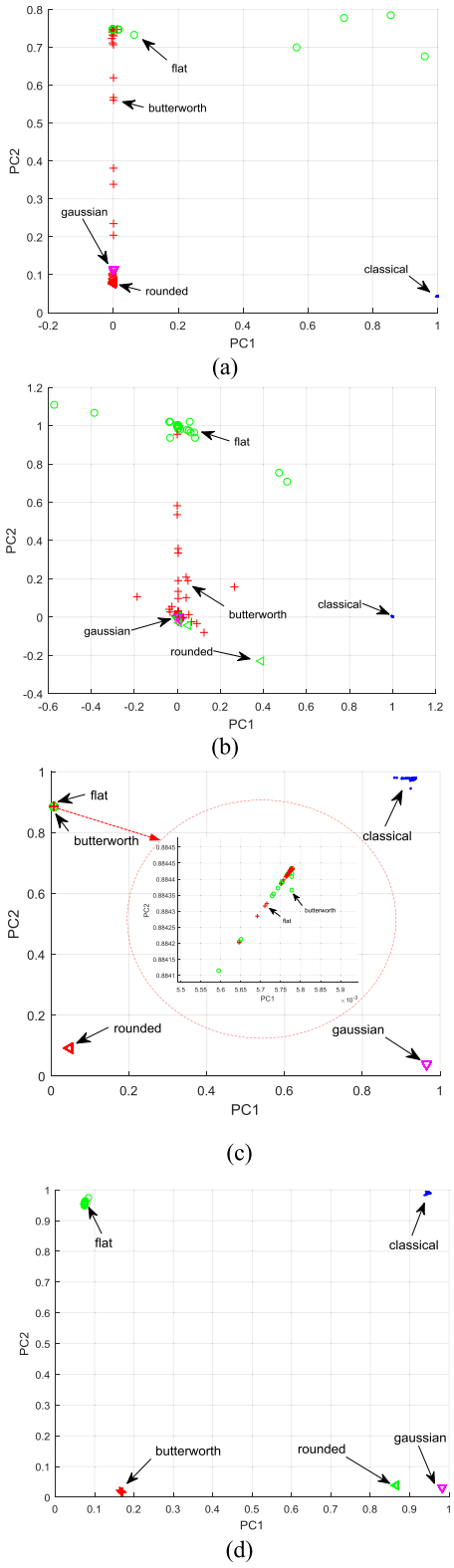

FIGURE 8. Two-dimensional feature distribution based on different methods under the simulation environment. (a) Based on the BP neural network method. (b) Based on the SVM method. (c) Based on RBF neural network method. (d) Based on this paper method.

TABLE 1. Comparison of correct recognition rates of four different methods under simulation environment.

Channel / Recognition rate / Classifier type	Classical fading channel	Flat fading channel	Rayleigh Gaussian channel	Rounded fading channel	Butterworth fading channel	Five kinds channel
BP neural network method	100%	98%	42%	56%	67%	72.6%
SVM method	100%	94%	96%	53%	69%	82.4%
RBF neural network method	100%	79%	100%	100%	58%	87.4%
This paper methods	100%	100%	100%	100%	100%	100%

TABLE 2. Confusion matrix of the channel scenario recognition on deep learning under physical platform.

Confusion matrix		Identify channel type				
		Classical	Flat	Gaussian	Rounded	Butterworth
Actual channel type	Classical	1.00	0.00	0.00	0.00	0.00
	Flat	0.00	1.00	0.00	0.00	0.00
	Gaussian	0.00	0.00	0.97	0.03	0.00
	Rounded	0.00	0.00	0.02	0.98	0.00
	Butterworth	0.00	0.00	0.00	0.00	1.00

TABLE 3. Comparison of correct recognition rates of four different methods under physical platform.

Channel / Recognition rate / Classifier type	Classical fading channel	Flat fading channel	Rayleigh Gaussian channel	Rounded fading channel	Butterworth fading channel	Five kinds channel
BP neural network method	100%	97%	40%	52%	57%	69.2%
SVM method	100%	89%	90%	51%	63%	78.9%
RBF neural network method	100%	92%	85%	86%	77%	80.0%
This paper methods	100%	100%	97%	98%	100%	99.2%

B. EXPERIMENT PLATFORM AND RESULTS

To further verify the accuracy of the proposed method, the author builds a comprehensive platform for the wireless channel scenario simulation was developed and analyzed. The application value of the method was further verified. A photograph of the comprehensive analysis test physical platform is shown in Fig.9. An analog signal generator and a vector signal generator were used to generate low-frequency signals and radio frequency signals, respectively. The signal analyzer conducted Doppler translation monitoring for the generated RF signal. A sub-5 GHz radio channel emulator with a bandwidth of 150 MHz, including eight input ports and eight output ports was employed. A radiofrequency (RF) down converter was combined with a 1-to-8 RF splitter in one module. Moreover, an RF upconverter was combined with one 8-to-1 RF combiners in another module, as shown in Fig.9. The frequency response of the channel simulator was recorded using a vector network analyser. The tested wireless channel data were imported into the computer processor to verify the recognition effect of the proposed method.

The test platform was used to test the signals of different wireless channel scenarios, using the autocorrelation function method to extract the parameters.

Fig.10 shows the extracted characteristic parameters in different Rayleigh channels through a physical platform. According to the extracted feature parameters, the proposed feature extraction method in this paper is still effective even in the actual simulation channel platform. The method can extract the characteristic parameters of different wireless channel scenarios. The characteristic parameters are

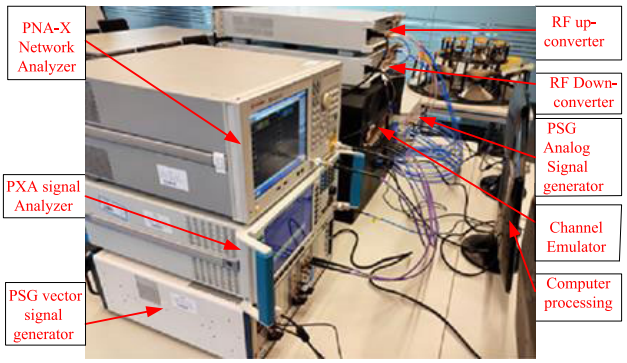

FIGURE 9. Channel scenario and analysis test physical platform.

significantly different in different channel scenarios. Moreover, the extracted feature parameters can also be used as the training data of the DBN.

The DBN was trained and tested using the test data. The relevant parameter settings were the same as those described in Sections A-C). The results were compared with those of the BP method, SVM method, and RBF method. The two-dimensional feature distribution corresponding to the wireless channel scene recognition results is shown in Fig.11.

Fig.11 (a) shows the two-dimensional feature distribution diagram of the scene recognition results obtained by using the BP neural network. As shown in Fig.11 (a), the curves for the Gaussian and Rounded channel are overlapped, indicating these channels cannot be well differentiated using the BP neural method. Moreover, the flat channel and the Butterworth channel are overlapped to a certain extent, indicating that the

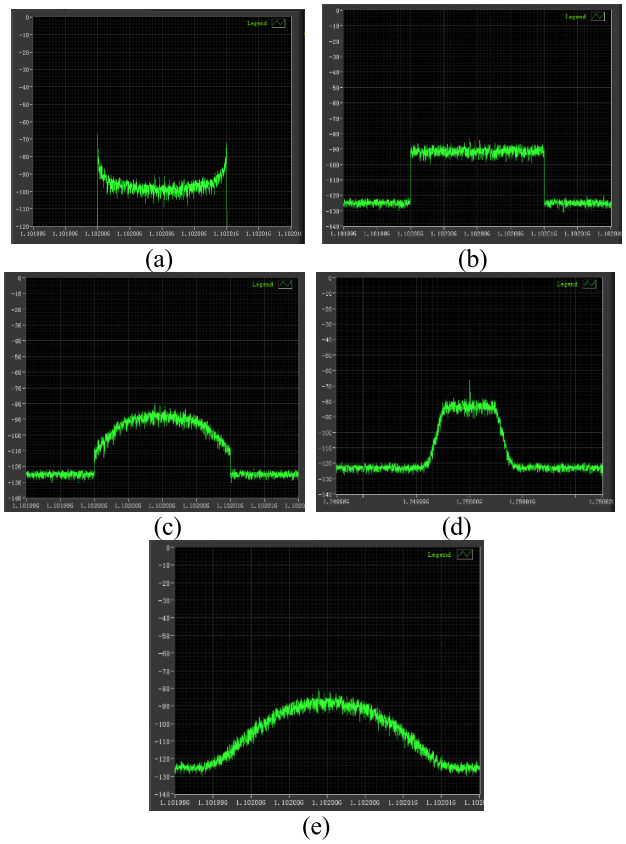

FIGURE 10. The extracted feature parameters from the physical platform. (a) PSD in the Classical fading channel. (b) PSD in Flat fading channel. (c) PSD in Gaussian fading channel. (d) PSD in Butterworth fading channel. (d) PSD in Rounded fading channel.

neural network method exhibits a mediocre performance in the recognition task. The platform test results are similar to the simulation results.

Fig.11 (b) shows the application effect of applying the SVM method in the scene recognition task. The four channels exhibit varying degrees of overlap, with considerable overlap between the Gaussian and rounded channels. This finding indicates that the BP method cannot well distinguish the Gaussian channel from the round and Butterworth channels.

Fig.11 (c) shows the two-dimensional feature distribution diagram of the scene recognition based on the RBF neural network. The RBF method can effectively identify the classical and Gaussian channels. However, a critical overlap occurs between the flat channel and the Butterworth channel. This method cannot effectively identify the two-channel scenarios.

Fig.11 (d) shows the two-dimensional feature distribution diagram for the proposed method. The two-dimensional features for different channel scenes exhibit a notable differentiation. Only a small amount of overlap can be noted between the Gaussian and rounded channels.

Table 2 presents the confusion matrix of the recognition results for the proposed method. The proposed method can accurately identify the scenes for the five channels when using the physical platform, with an extremely high correct recognition rate.

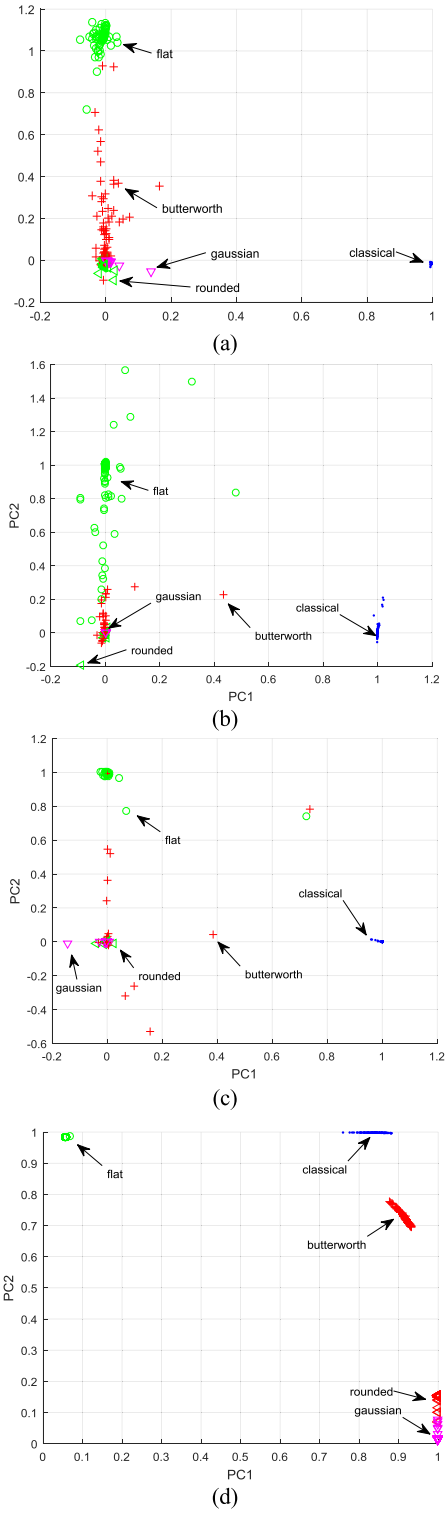

FIGURE 11. Two-dimensional feature distribution pertaining to different methods, obtained using the physical platform (a) Used BP neural network method (b) Used SVM method (c) Used RBF neural network method (d) Proposed method.

Table. 3 presents the correct recognition rates for four different scene recognition methods. The classical fading channel can be identified through the four methods, with an accuracy rate of 100%. This result indicates that the four

methods can well identify the Gaussian fading channel. For the flat and Butterworth fading channels, the recognition rate of the proposed method is 100%, even though the recognition rates for the other three conventional methods are low. The results indicate that for these two channels, the representation based on deep learning is the highest performing approach. For the Rayleigh Gaussian channel and Butterworth fading channel, the recognition rate of the proposed method is higher than that of the other three methods. The experimental results show that compared with other methods, the proposed deep learning method has a stronger learning ability for wireless channel scenarios. This method can more effectively realize the feature extraction and classification.

As shown in Table.3, the proposed method can realize the most effective channel scene recognition. The overall correct recognition rate of the proposed method is 99.2%. The BP method exhibits the worst recognition effect, with a correct recognition rate of only 69.2%. The results of the SVM and RBF are comparable, with a correct recognition rate of 82.4% and 87.4%, respectively. In the wireless channel scenarios with fast time-variations, large broadband, and multiple dimensions, the traditional methods cannot achieve a high recognition accuracy. Overall, the proposed identification method exhibits the strongest recognition ability.

V. CONCLUSION

This paper proposes a wireless channel scene recognition method based on feature parameter extraction and deep learning. The autocorrelation function is used to extract the characteristic parameters of a wireless channel scene. The windowing and overlap techniques are adopted to realize the process of time-frequency transformation. Normalized pre-processing is recognized in the frequency domain, and the satisfactory characteristic parameters are obtained from the wireless channel. A deep learning algorithm with a robust taxonomy ability is applied to realize the wireless channel scene recognition. A hybrid model is built by using the restricted Boltzmann machine of the DBN. The CD-k learning algorithm is used to initialize the network parameters, and the up-down-optimization algorithm is used to optimize the identification weights and offset parameters. The theoretical simulation results demonstrate the correctness and accuracy of the method. Finally, a wireless channel scene recognition platform is built by combining hardware and software. The experimental results show that the proposed algorithm exhibits high performance in the wireless channel scene recognition task. The proposed method can accurately identify the different channel scenes and thereby demonstrates high engineering application value.

REFERENCES

[1] L. Liu, G. Han, S. Chan, and M. Guizani, "An SNR-assured anti-jamming routing protocol for reliable communication in industrial wireless sensor networks," *IEEE Commun. Mag.*, vol. 56, no. 2, pp. 23–29, Feb. 2018.

[2] H. Rong and M.-R. Chen, "Influence and countermeasures on the ship-borne communication equipment of naval field complex electromagnetic environment," in *Proc. 11th Int. Symp. Distrib. Comput. Appl. Bus., Eng. Sci.*, Oct. 2012, pp. 345–347.

[3] X. Li, S. Jin, H. A. Suraweera, J. Hou, and X. Gao, "Statistical 3-D beamforming for large-scale MIMO downlink systems over Rician fading channels," *IEEE Trans. Commun.*, vol. 64, no. 4, pp. 1529–1543, Apr. 2016.

[4] D. A. Basnayaka and H. Haas, "Overcoming large-scale fading in cellular systems with network coordination," *IEEE Trans. Commun.*, vol. 62, no. 7, pp. 2589–2601, Jul. 2014.

[5] R. M. Gutierrez, H. Yu, Y. Rong, and D. W. Bliss, "Comparison of UAS-to-ground small-scale fading in residential and mountainous desert terrains," *IEEE Trans. Veh. Technol.*, vol. 68, no. 10, pp. 9348–9358, Oct. 2019.

[6] B. Zhang, Z. Zhong, R. He, F. Tufvesson, and B. Ai, "Measurement-based multiple-scattering model of small-scale fading in high-speed railway cutting scenarios," *IEEE Antennas Wireless Propag. Lett.*, vol. 16, pp. 1427–1430, 2017.

[7] F. Gao, X. Feng, and Y. Zheng, "Micro-Doppler photoacoustic effect and sensing by ultrasound radar," *IEEE J. Sel. Topics Quantum Electron.*, vol. 22, no. 3, pp. 152–157, May 2016.

[8] J. Ran, Y. Zhang, X. Chen, and H. Chen, "Frequency mixer based on Doppler effect," *IEEE Microw. Wireless Compon. Lett.*, vol. 28, no. 1, pp. 43–45, Jan. 2018.

[9] D. Gesbert and P. Duhamel, "Unbiased blind adaptive channel identification and equalization," *IEEE Trans. Signal Process.*, vol. 48, no. 1, pp. 148–158, Jan. 2000.

[10] W. Xu and S. A. R. Zekavat, "Novel high performance MIMO-OFDM based measures for NLOS identification in time-varying frequency and space selective channels," *IEEE Commun. Lett.*, vol. 16, no. 2, pp. 212–215, Feb. 2012.

[11] B. Yang, "Projection approximation subspace tracking," *IEEE Trans. Signal Process.*, vol. 43, no. 1, pp. 95–107, Jan. 1995.

[12] Y. Wen, S. C. Chan, and K. L. Ho, "Robust subspace tracking based blind channel identification in impulsive noise environment," in *Proc. 11th Eur. Signal Process. Conf.*, Toulouse, France, 2002, pp. 1–4.

[13] X. Zhang, F. Gao, R. Chai, and T. Jiang, "Matched filter based spectrum sensing when primary user has multiple power levels," *China Commun.*, vol. 12, no. 2, pp. 21–31, Feb. 2015.

[14] H. Gu, Y. Wang, S. Hong, and G. Gui, "Blind channel identification aided generalized automatic modulation recognition based on deep learning," *IEEE Access*, vol. 7, pp. 110722–110729, 2019.

[15] F. Carpi, L. Davoli, M. Martalo, A. Cilfone, Y. Yu, Y. Wang, and G. Ferrari, "RSSI-based methods for LOS/NLOS channel identification in indoor scenarios," in *Proc. 16th Int. Symp. Wireless Commun. Syst. (ISWCS)*, Oulu, Finland, Aug. 2019, pp. 171–175.

[16] M. R. D. Rodrigues, "Multiple-antenna fading channels with arbitrary inputs: Characterization and optimization of the information rate," *IEEE Trans. Inf. Theory*, vol. 60, no. 1, pp. 569–585, Jan. 2014.

[17] R. H. Clarke, "A statistical theory of mobile-radio reception," *Bell Syst. Tech. J.*, vol. 47, no. 6, pp. 957–1000, Jul. 1968.

[18] W. C. Jakes, *Microwave Mobile Communications*. Piscataway, NJ, USA: IEEE Press, 1994.

[19] M. F. Pop and N. C. Beaulieu, "Limitations of sum-of-sinusoids fading channel simulators," *IEEE Trans. Commun.*, vol. 49, no. 4, pp. 699–708, Apr. 2001.

[20] M. Sharma and R. Nath, "An improved sum-of-sinusoids based simulation model for Rayleigh fading channel," in *Proc. 3rd Int. Conf. Comput., Commun., Control Inf. Technol. (C IT)*, Hooghly, India, Feb. 2015, pp. 1–3.

[21] P. Hoeher, "A statistical discrete-time model for the WSSUS multipath channel," *IEEE Trans. Veh. Technol.*, vol. 41, no. 4, pp. 461–468, Nov. 1992.

[22] R. W. Klein, M. A. Temple, and M. J. Mendenhall, "Application of wavelet-based RF fingerprinting to enhance wireless network security," *J. Commun. Netw.*, vol. 11, no. 6, pp. 544–555, Dec. 2009.

[23] S. Y. Han, N. B. Abu-Ghazaleh, and D. Lee, "Efficient and consistent path loss model for mobile network simulation," *IEEE/ACM Trans. Netw.*, vol. 24, no. 3, pp. 1774–1786, Jun. 2016.

[24] J. L. Cornette, "Gauss-Vanícek and Fourier transform spectral analyses of marine diversity," *Comput. Sci. Eng.*, vol. 9, no. 4, pp. 61–63, Jul. 2007.

[25] S. Koganezawa, S. Tsuda, H. Tani, R. Lu, and N. Tagawa, "Frequency analysis of disturbance torque exerted on a carriage arm in hard disk drives using Hilbert–Huang transform," *IEEE Trans. Magn.*, vol. 54, no. 11, pp. 1–6, Nov. 2018.

[26] D. Tao, X. Li, X. Wu, and S. J. Maybank, "General tensor discriminant analysis and Gabor features for gait recognition," *IEEE Trans. Pattern Anal. Mach. Intell.*, vol. 29, no. 10, pp. 1700–1715, Oct. 2007.

[27] J. A. Garzon-Guerrero, D. P. Ruiz, and M. C. Carrion, "Classification of geometrical targets using natural resonances and principal components analysis," *IEEE Trans. Antennas Propag.*, vol. 61, no. 9, pp. 4881–4884, Sep. 2013.
[28] W. Wang, Z. Sun, S. Piao, B. Zhu, and K. Ren, "Wireless physical-layer identification: Modeling and validation," *IEEE Trans. Inf. Forensics Security*, vol. 11, no. 9, pp. 2091–2106, Sep. 2016.
[29] P. Lingras, M. Chen, and D. Miao, "Rough cluster quality index based on decision theory," *IEEE Trans. Knowl. Data Eng.*, vol. 21, no. 7, pp. 1014–1026, Jul. 2009.
[30] J. W. Robertson, K. B. Englehart, and E. J. Scheme, "Effects of confidence-based rejection on usability and error in pattern recognition-based myoelectric control," *IEEE J. Biomed. Health Informat.*, vol. 23, no. 5, pp. 2002–2008, Sep. 2019.
[31] Y. Li, J. Zhang, P. Tang, and L. Tian, "Clustering in the wireless channel with a power weighted statistical mixture model in indoor scenario," *China Commun.*, vol. 16, no. 7, pp. 83–95, Jul. 2019.
[32] L. Yuan, Y. He, J. Huang, and Y. Sun, "A new neural-network-based fault diagnosis approach for analog circuits by using kurtosis and entropy as a preprocessor," *IEEE Trans. Instrum. Meas.*, vol. 59, no. 3, pp. 586–595, Mar. 2010.
[33] P. A. Gutierrez, C. Hervas-Martinez, and F. J. Martinez-Estudillo, "Logistic regression by means of evolutionary radial basis function neural networks," *IEEE Trans. Neural Netw.*, vol. 22, no. 2, pp. 246–263, Feb. 2011.
[34] L. Shi, Y. He, B. Li, Y. Wu, Y. Huang, and T. Cheng, "On-line measurement of dynamic tilt angle by compensating gyroscope drift error," *IEEE Trans. Instrum. Meas.*, vol. 68, no. 9, pp. 3244–3252, Sep. 2019.
[35] T. Wang, Y. He, T. Shi, J. Tong, and B. Li, "Transformer health management based on self-powered RFID sensor and multiple kernel RVM," *IEEE Trans. Instrum. Meas.*, vol. 68, no. 3, pp. 818–828, Mar. 2019.

SHUGUANG NING received the M.Sc. degree in electrical theory and advanced technology from the Hefei University of Technology, Hefei, China, in 2019, where he is currently pursuing the Ph.D. degree in electrical engineering. His current research interests include wireless communication, deep learning, intelligent perception, and its application in power internet of things.

YIGANG HE received the M.Sc. degree in electrical engineering from Hunan University, Changsha, China, in 1992, and the Ph.D. degree in electrical engineering from Xi'an Jiaotong University, Xi'an, China, in 1996. His teaching and research interests include power electronic circuit theory and its applications, testing and fault diagnosis of analog and mixed-signal circuits, electrical signal detection, smart grid, satellite communication monitoring, and intelligent signal processing. He has published some 300 journal and conference papers which were included more than 1000 times in Science Citation Index of American Institute for Scientific Information in the aforementioned areas and several chapters in edited books. He has been on the Technical Program Committees of a number of international conferences. He was a recipient of a number of national and international awards, prizes, and honors. For example, he was the winner of national outstanding youth science fund, China national excellent science and technology worker.

LIFEN YUAN received the Ph.D. degree in electrical engineering from Hunan University, China, in 2011. From 2003 to 2010, she worked with Hunan Normal University. Since 2013, she has been a Professor with the Hefei University of Technology, Hefei, Anhui, China. Her current research interests include circuit diagnosis, wireless communication, advanced signal processing, and its application.

YUAN HUANG received the B.S. degree from the Hefei University of Technology, Hefei, Anhui, China, in 2016, where he is currently pursuing the Ph.D. degree in electrical engineering. His current research interests include digital signal processing, wireless communication, deep learning, and compressed sensing.

SHUDONG WANG (Graduate Student Member, IEEE) received the B.S. degree in automation from Anhui Polytechnic University, Wuhu, China, in 2015. He is currently pursuing the Ph.D. degree in electrical engineering with the Hefei University of Technology, Hefei, China. His current research interests include electric power equipment insulation online monitoring and fault diagnosis.

TONGTONG CHENG received the B.S. degree from the Hefei University of Technology, Hefei, Anhui, China, in 2016, where he is currently pursuing the Ph.D. degree in electrical engineering. His current research interests include intelligent information processing, wireless communication, and smart grid technology.

YONGBO SUI received the B.E. degree in electrical engineering from Xiangtan University, Xiangtan, Hunan, China, in 2014. He is currently pursuing the Ph.D. degree with the Hefei University of Technology, Hefei, Anhui, China. His research interests include intelligent algorithms and wireless communication channels.